Korean J. Chem. Eng., 36(12), 2110-2117 (2019)
DOI: 10.1007/s11814-019-0386-8

pISSN: 0256-1115
eISSN: 1975-7220

Green and low-cost preparation of CIGSe thin film by a nanocrystals ink based spin-coating method

Trang Thi Thuy Le, Nam Le, Mohan Reddy Pallavolu, Yoonchang Jeon, Dong-seob Jeong, Babu Pejjai, Vasudeva Reddy Minnam Reddy, Nguyen Tam Nguyen Truong, and Chinho Park†

School of Chemical Engineering, Yeungnam University, 280 Dae-dong, Gyeongsan 38541, Korea
(*Received 3 June 2019 • accepted 4 September 2019*)

Abstract−An "ink" solution based process, using spin-coating technique, followed by annealing in selenium environment with different temperature programs was utilized to prepare CIGSe thin films. Herein, the $CuIn_{0.7}Ga_{0.3}Se_2$ nanocrystals were synthesized using ethanol - a "green" solvent. Three different solvents: 2-propanol, 2-methoxyethanol, and their 2 : 1 mixture (v/v ratio), were investigated as a dispersion medium for the as-synthesized CIGSe nanocrystals to form a stable ink solution. The last one- a mixture of 2-propanol : 2-methoxyethanol=2 : 1 (v/v), was found to be the most suitable. Furthermore, the influences of various annealing modes on the CIGSe grain size and density in the resulting film were also studied. The as-prepared CIGSe thin film was around 1 μm thick and possessed a tetragonal structure. A newly developed cheaper and "greener" non-vacuum process was applied successfully from the synthesis of nanocrystals to the formation of ink solution, and produced high quality thin films; this opens a new route to the cost-competitive commercialization of CIGSe thin film solar cells.

Keywords: CIGSe Compound, Solution Based Process, Spin-coating Method, CIGSe Thin Film Solar Cell

INTRODUCTION

Chalcopyrite $CuIn_xGa_{1-x}Se_2$ (CIGSe) compounds have been known as semiconducting materials that have a direct band gap in the range of 1.0-1.7 eV and high optical absorption coefficient $\alpha > 10^5\ cm^{-1}$ [1,2]. Therefore, much effort has been made to prepare CIGSe thin film as an effective light-absorbing layer for thin film solar cell industry, and the efficiency of CIGSe solar cell has reached 23.35% recently [3]. However, the cost of fabrication is very high and energy consumption is significant, because these thin films were prepared by vacuum-based deposition methods such as sputtering [4-8] and co-evaporation [9-14] which require sophisticated equipment. On the other hand, the impurities from the substrates also significantly affect the performance of thin film solar cells, which results from high temperature employed in vacuum-based techniques.

To minimize these issues, many studies have been done on non-vacuum methods such as printing [15-18], dip coating [19], drop casting [20], supersonic kinetic spraying [21,22], spin coating [23, 24], electro-deposition [25,26], doctor blading [27,28], solvothermal [29], milling process [30] and hot injection [31] to develop a low-cost manufacturing method of CIGSe thin film. However, these methods are solution-based processes typically involving toxic organic solvents such as trioctylphosphine, tributylphosphine, polyetheramine, ethylenediamine and hydrazine (very toxic if inhaled), which are harmful to the environment as well as people's health, or the solvents having a high boiling point such as oleyamine, octadecane, polyetheramine resulting in high reaction temperatures up to 280 °C and producing carbon residues in the resulting thin films.

In this paper, we present a new methodology to prepare thin films from CIGSe nanocrystals by spin coating method. Herein, CIGSe nanocrystals were synthesized using "green" solvents - ethanol by sonochemistry. The fabrication of a thin film by spin coating is challenged by the need to find a suitable but less toxic solvent compared to hydrazine as previous reports, into which the as-synthesized CIGSe nanocrystals could be well dispersed resulting in stable "ink" solutions [32,33]. Furthermore, in the manufacture of CIGSe thin film solar cell, a grain size is expected in the range 1-2 μm. Thus, we also attempted to optimize the annealing step to improve CIGSe grain size of resulting thin film. Note that no long hydrocarbon chains containing ligands were applied in any of the processes involved, so this is a surfactant-free procedure.

According to a literature survey [34-36], the composition of $CuIn_xGa_{1-x}Se_2$ compound should be $CuIn_{0.7}Ga_{0.3}Se_2$ to give the best efficiency in CIGSe thin film solar cells. Therefore, in the present work, we targeted to prepare thin film from the as-synthesized $CuIn_{0.7}Ga_{0.3}Se_2$ nanocrystals.

EXPERIMENTAL DETAILS

All chemicals CuCl (99.99%), $InCl_3$ (99.999%), $Ga(NO_3)_3$. xH_2O (99.9%), Se (99.99%) sodium borohydride ($NaBH_4$), 2-propanol (C_3H_8O, 99.5%), ethyl alcohol (C_2H_5OH, 99.5 %) and 2-methoxyethanol ($C_3H_8O_2$, 99.3%) were products of Sigma Aldrich and used as-received. The applied equipment included a VCX 750 Sonic & Materials ultrasonic processor (P=300 W, f=20 kHz), a furnace machine (Lenton Thermal Designs) and a spin coater ACE-200.

1. Synthesis of CIGSe Nanocrystals

CIGSe nanoparticles were synthesized following the procedure that we reported previously [37]. Briefly, Se powder was dissolved in two beakers containing $NaBH_4/C_2H_5OH$ solution to form Se

†To whom correspondence should be addressed.
E-mail: chpark@ynu.ac.kr

precursor solution. When these reddish-brown solutions became transparent, gallium nitrate and indium chloride were loaded into each beaker separately, and at that time the solutions changed from transparent into the turbid colloidal solutions with yellow precipitates. Subsequently, these two colloidal solutions were mixed with each other, followed by adding copper chloride. The resulting deep black colloidal suspension was ultrasonicated 5 h at room temperature. The black precipitates were centrifuged, rinsed three times with distilled water and twice with ethanol, then dried at 50 °C for 7 h in drying oven.

2. Formation of Thin Film from a CIGSe Nanocrystals Ink Based Spin Coating Method

The thin film was fabricated by ink solution based coating method. To prepare an ink solution, we studied dispersing the as-synthesized nanocrystals in three different solvents: 2-propanol, 2-methoxyethanol and solvent mixture of 2-propanol and 2-meth- oxyethanol (2 : 1 v/v ratio). These mixtures were constantly stirred for 24 h, and then these colloidal solutions were kept stable for one month to observe the stability of ink solution. This step aims to find the suitable solvent as a medium of dispersion for CIGSe ink solution.

The as-prepared ink solution was coated on Mo-coated soda lime glass by spin coater (6,000 rpm, 40 s) to form thin film. The spin-coated films were then annealed under nitrogen and selenium atmosphere with various temperature programs to optimize grain size and density of the CIGSe thin film. The furnace machine is type of two zone furnace. Selenium powder was put in first zone and CIGSe film was in second zone. Temperature of first zone was always controlled at around 240 °C in all various annealing modes to selenium powder forming selenium vapor supplying to CIGSe film. In the second zone, the temperature program was changed in each annealing mode as follows:

Annealing mode 1:

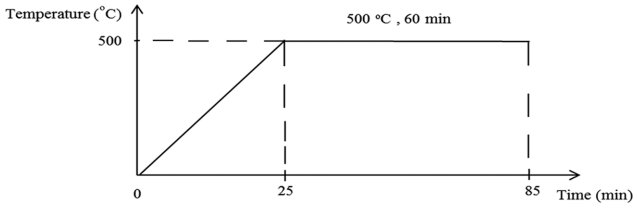

Annealing mode 2:

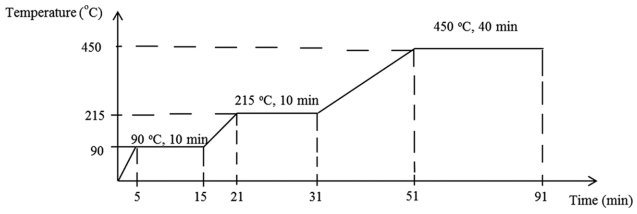

Annealing mode 3:

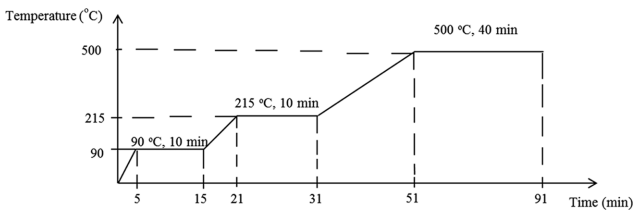

The products were analyzed by various techniques. Raman spectroscopy (XploRA plus Horiba), powder X-ray diffraction (XRD, PANalytical, X'Pert-PRO MPD) and thin film X-ray reflectometry (PANalytical, X'Pert-PRO) were used to characterize the crystal structure of the as-synthesized product. The XRD patterns were recorded using Cu/Kα radiation (λ=1.056). The Raman spectra were measured at room temperature using 532 nm Laser as an excitation light source. X-ray photoelectron spectroscopy (XPS) measurements were carried out on a Thermo scientific K-alpha spectrometer using Al Kα monochromatized radiation to investigate the valence states of the elements in the products. Inductively coupled plasma atomic emission spectroscopy (ICPS, ICPS 8100 Shimadzu system) was employed to analyze composition of elements in the as-synthesized products. Transmission electron microscopy (TEM, Philips CM-200) and scanning electron microscopy (SEM, Hitachi S-4800) were used to characterize the size and morphology of nanoparticles and thin film. The transmittance spectra were measured on a Cary 5000 UV-vis-NIR spectrophotometer (Varian) to calculate the band gap energy (E_g) of the as-synthesized CIGSe thin film. Hall effect measurement was carried out on Nanometrics hall measurement (HL5500) to characterize the electrical properties of the as-synthesized product.

RESULT AND DISCUSSION

1. Synthesis of CIGSe Nanocrystals

The structural properties of the as-synthesized products were analyzed by X-ray diffraction XRD. From XRD patterns in Fig. 1, we could easily observe that five main index planes of (112), (220), (312), (400) and (332) were obtained. These are typical planes for tetragonal structure as well as $CuIn_{0.7}Ga_{0.3}Se_2$ compound according to the reference JCPDS 035-1102. Besides, there are no signs of impurity in the overall XRD patterns, indicating only $CuIn_{0.7}Ga_{0.3}Se_2$ nanocrystals formed in the process. Raman spectroscopy was also applied to confirm the structure of the as-synthesized nanoparticles and detect the presence of any secondary phases. A mode peak in Fig. 2 appears clearly at 176-177 cm^{-1}, which is a strong peak generally observed in the Raman spectrum of $Cu(In_xGa_{1-x})Se_2$ compound. This mode was rather higher than the 172-174 cm^{-1} for pure $CuInSe_2$ resulting from the presence of gallium element [38,39]. Besides, there was no shoulder peak of Cu_xSe centered at around 260 cm^{-1}, indicating that Cu_xSe did not involve as an impurity in the as-synthesized products. This matches well with the above XRD result.

The morphology and size of the CIGSe nanoparticles were meas0-ured by scanning electron microscopy (SEM) and transmission electron microscopy (TEM) in Fig. 3. The images show that the as-synthesized nanoparticles had a quasi-spherical shape and uniform size of around 10 nm.

X-ray photoelectron spectroscopy (XPS) was used to investigate the valence states and composition of the elements in the as-synthesized. The Cu 2p, In 3d, Ga 2p and Se 3d core levels were studied, respectively. Fig. 4 shows that their obtained binding energies are in accordance with those reported for CIGSe compounds [40-42]. Furthermore, the Cu 2p core level spectrum in Fig. 4(a) exhibits that the binding energies for Cu $2p_{1/2}$ and Cu $2p_{3/2}$ are

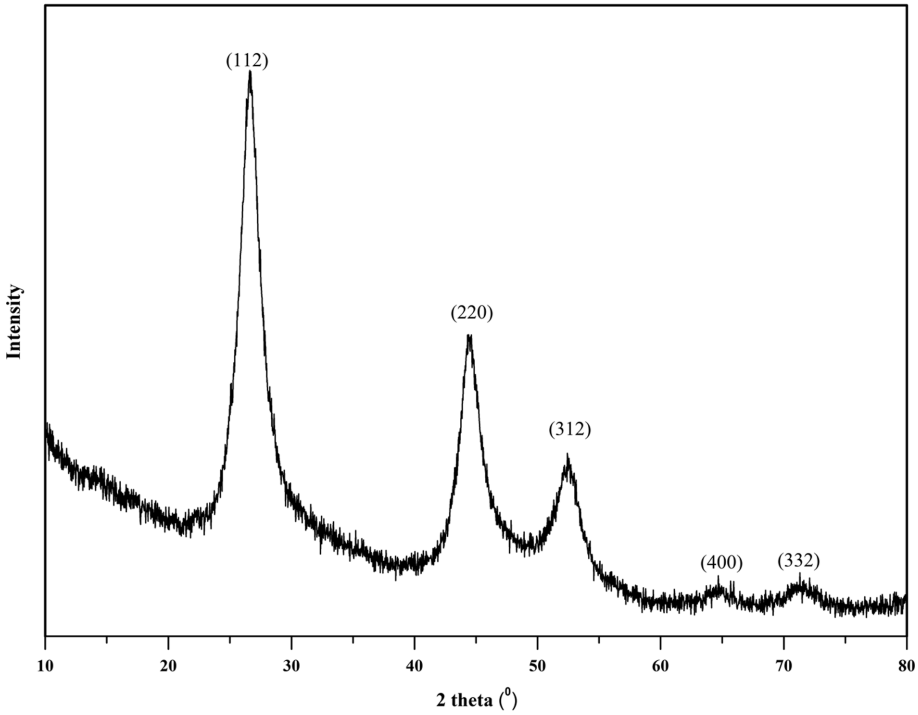

Fig. 1. XRD pattern of the CIGSe nanocrystals prepared with 5 h ultrasonification time.

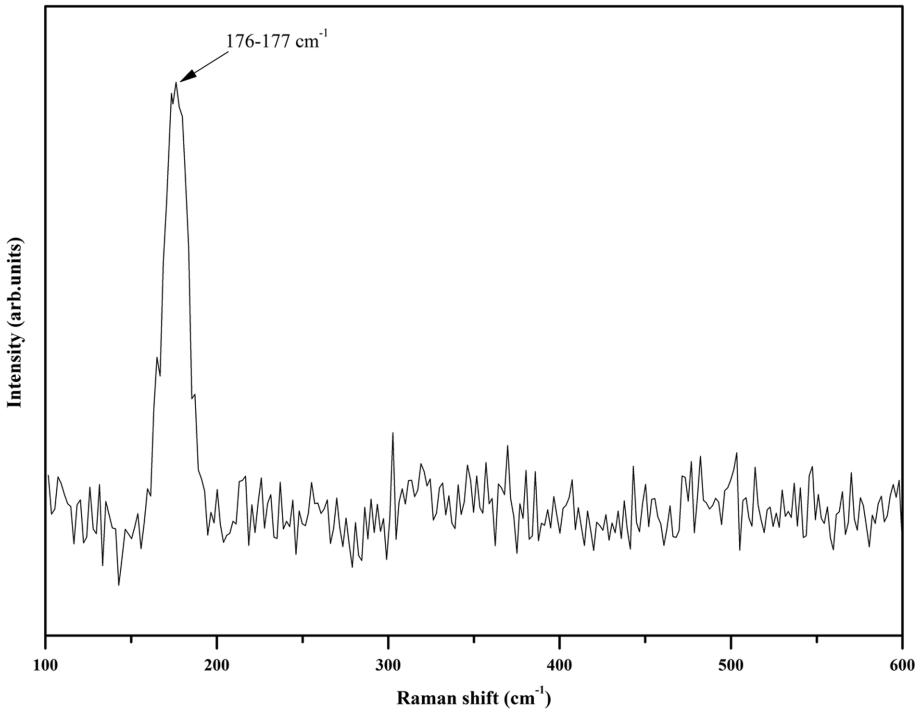

Fig. 2. Raman spectra of the as-synthesized CIGSe nanocrystals with 5 h ultrasonification time.

951.88 eV and 932.18 eV, respectively, and the full width at half maximum for peak Cu $2p_{3/2}$ is only 1.22 eV. These values match well with values reported for Cu(I) 2p binding energy [43]. On the other hand, there was no typical shoulder peak of Cu^{2+} detected in the obtained spectrum. Hence, it can be concluded that only Cu^{+} exists in the as-synthesized products.

The stoichiometry of the as-synthesized products was determined by applying Vegard's law [44,45] to their XRD data obtained. ICPS and XPS results were also evaluated for this purpose. Table 1 reveals that there are small deviations from the obtained results.

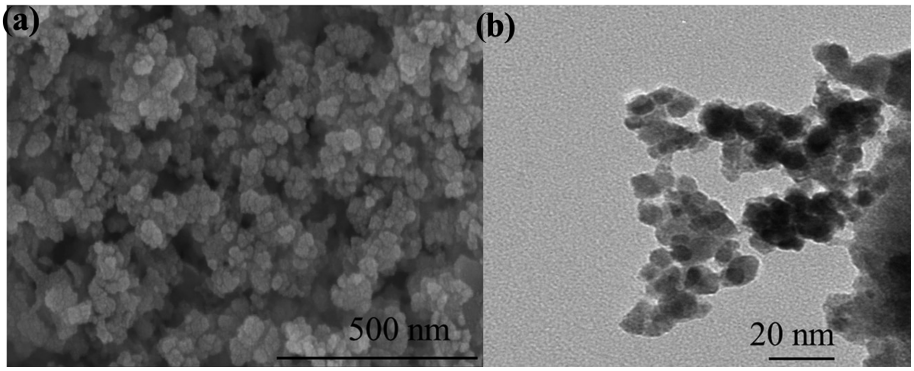

Fig. 3. SEM (a) and TEM (b) images of the CIGSe nanocrystals with 5 h ultrasonification time.

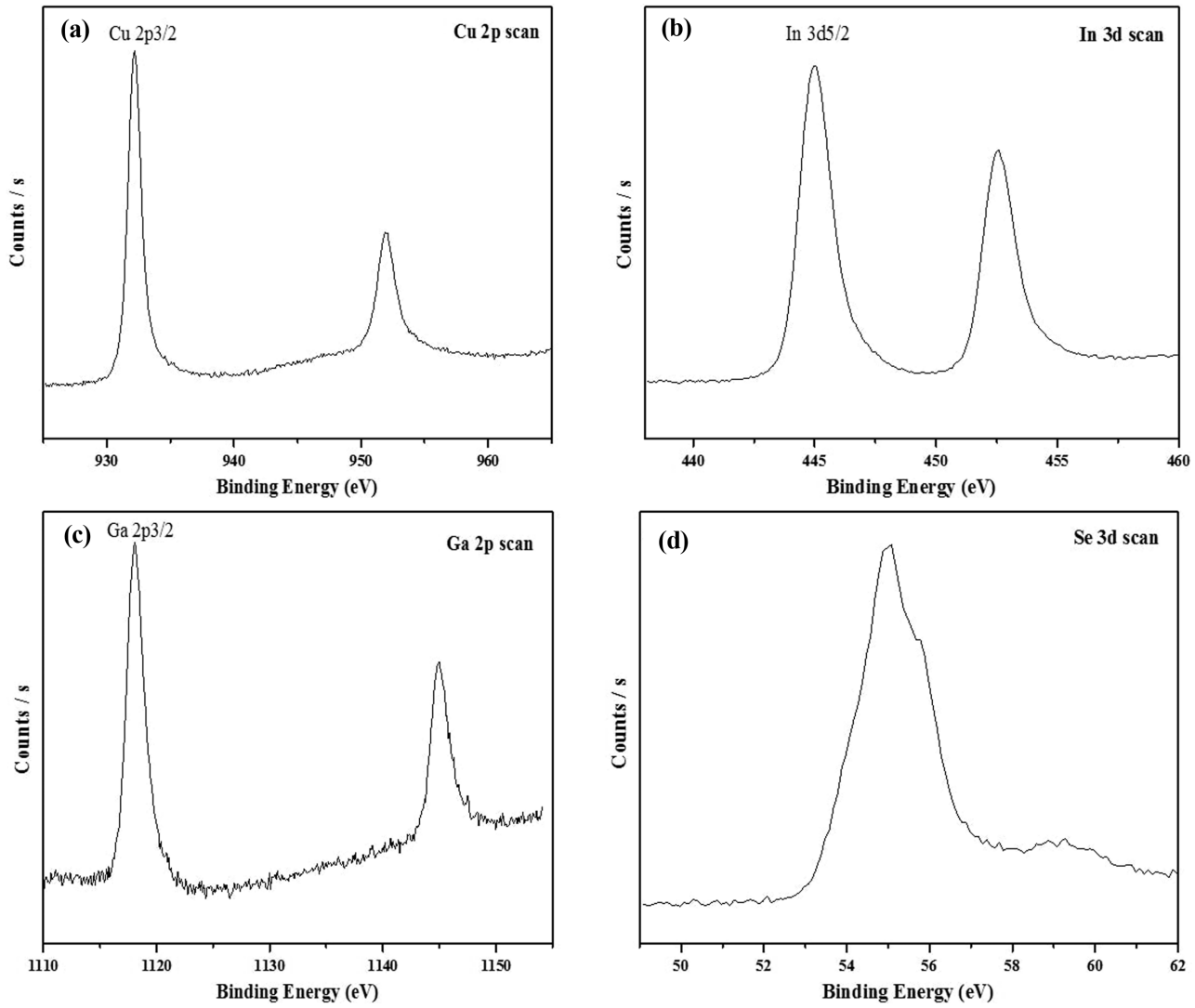

Fig. 4. XPS core-level spectra: Cu 2p (a), In 3d (b), Ga 2p (c), and Se 3d (d) of as-synthesized $CuIn_{0.7}Ga_{0.3}Se_2$ nanocrystals.

Table 1. Chemical composition of the as-synthesized CIGSe compounds

Target compound	Composition calculated by Vegard's law (atomic ratio, Cu/In/Ga/Se)	Composition measured by XPS (atomic ratio, Cu/In/Ga/Se)	Composition measured by ICPS (atomic ratio, Cu/In/Ga/Se)
$CuIn_{0.7}Ga_{0.3}Se_2$	1 : 0.67 : 0.33 : 2	1 : 0.82 : 0.37 : 1.81	1 : 0.84 : 0.29 : 1.89

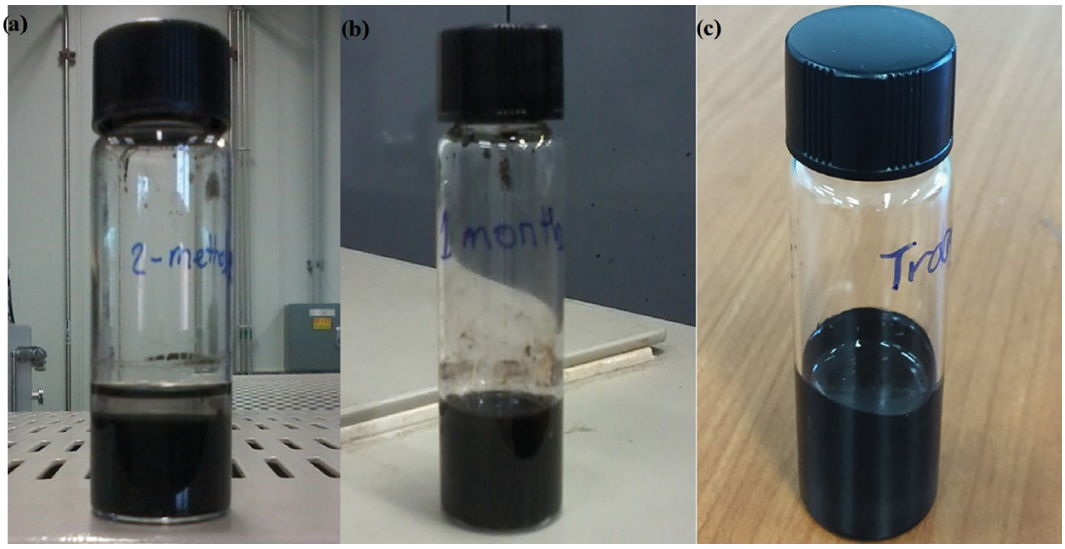

Fig. 5. The images of colloidal solutions with different dispersion mediums: 2-propanol (a), 2-methoxyethanol (b) and solvent mixture of 2-propanol and 2-methoxyethanol (c) after being kept in 1 month.

Fig. 6. The images of the spin coated films by 2-propanol solvent based ink solution (a), and solvent mixture based ink solution (b).

However, we could see that the composition of elements is close to the target compound ($CuIn_{0.7}Ga_{0.3}Se_2$).

2. Formation of Thin Film from a CIGSe Nanocrystals Ink Based Spin Coating Method

The images in Fig. 5 reveal the level of stability of each solution (after being kept stable in one month) when the as-synthesized CIGSe nanocrystals were dispersed in three different solvents: 2-propanol, 2-methoxyethanol and solvent mixture of 2-propanol and 2-methoxyethanol (2 : 1 v/v ratio).

Fig. 5(a) shows that there is a slight agglomeration of colloids in 2-methoxyethanol solvent. However, these colloids seem to be dispersed well in 2-propanol solvent and solvent mixture of 2-propanol : 2-methoxyethanol; hence, the ink solutions were stable as shown in Fig. 5(b) and (c). This might be because the value of surface tension of 2-methoxyethanol (42.8) is higher than 2-propanol (23.3); thus, it is more difficult to disperse CIGSe nanocrystals in 2-methoxyethanol solvent. However, the spin coated film from the 2-propanol solvent based ink solution was not uniform (Fig. 6(a)), and a little bit of solvent still remained on film even if we increased the speed to 8,000 rpm, perhaps because the value of viscosity of 2-propanol was high (2.04 cP). Indeed, for solvent mixture of 2-propanol and 2-methoxyethanol (the viscosity is 1.72 cP), the film formed really smooth and no solvent remained after spin coating (Fig. 6(b)). Therefore, this solvent mixture was chosen as dispersion medium to form CIGSe ink solution and all the thin films were deposited by spin coating from this ink solution used for the annealing step.

Three different annealing modes were conducted to optimize grain size as well as density of the CIGSe thin film. For the thin film of the first annealing mode, we could easily observe that the size of the as-synthesized CIGSe nanoparticles in thin film increased significantly, but the density of thin film was not good, as many voids appeared in the film (Fig. 7). Maybe it is due to the rapid evaporator of the solvent at 500 °C leaving many holes in thin film. However, in the second annealing mode, the image in Fig. 9 shows that the density of film was better than the first annealing mode. This may be explained as follows: temperature was held at 90 °C in first 10 min, helping the evaporation of solvent occurring slowly;

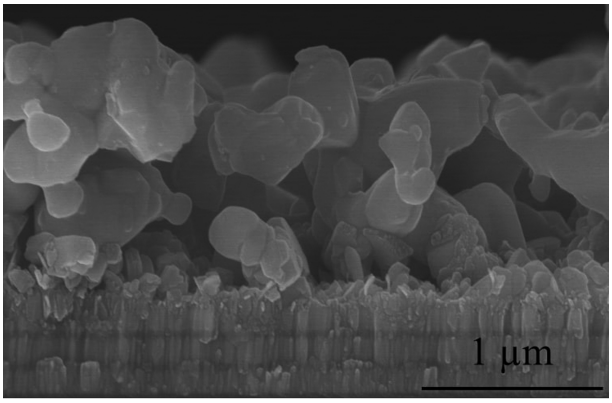

Fig. 7. Cross-section SEM image of CIGSe thin film with the first annealing mode.

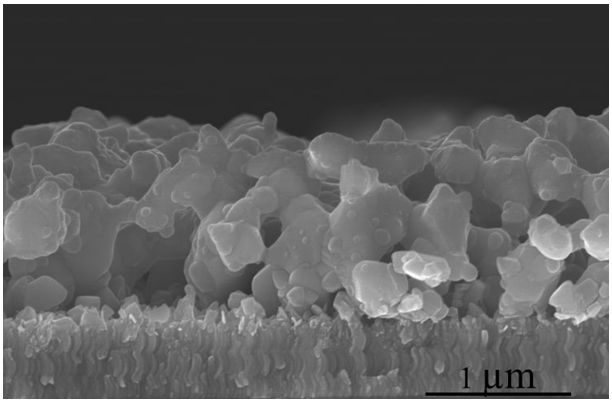

Fig. 9. Cross-section SEM image of CIGSe thin film with the third annealing mode.

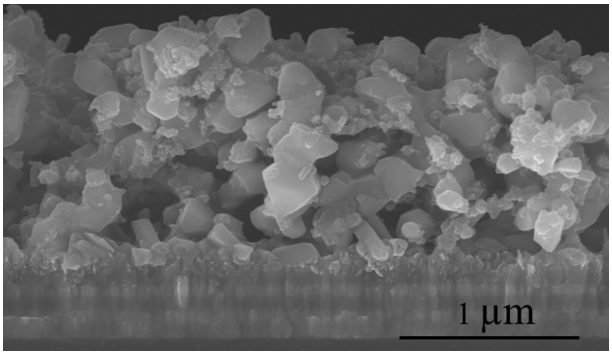

Fig. 8. Cross-section SEM image of CIGSe thin film with the second annealing mode.

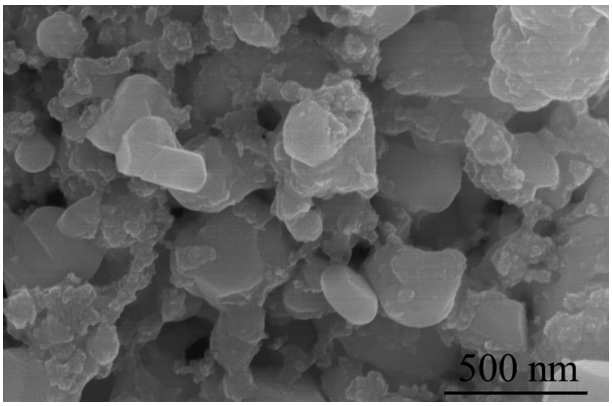

Fig. 10. Surface SEM image of CIGSe thin film with the third annealing mode.

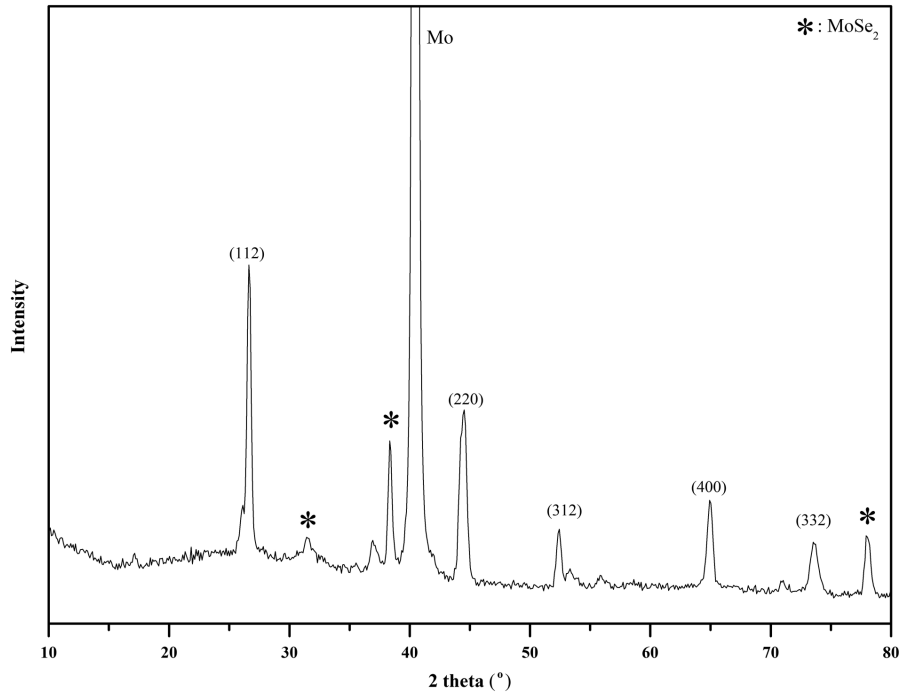

Fig. 11. XRD pattern of CIGSe thin film after being annealed with the third annealing mode.

besides, temperature was kept at 215 °C in next 10 min favoring the gradual melting of selenium in CIGSe compound, and thus had the time to stick nanoparticles together. However, temperature of 450 °C in the last 40 min was not enough to expand the size of CIGSe nanoparticles as the first annealing mode. Indeed, for the thin film of the third annealing mode, when temperature of the last 40 min was changed into 500 °C, the size of CIGSe nanoparticles increased much more (Fig. 9). Fig. 9 also shows the thickness of thin film to be about 1 μm; this is in range of thickness of CIGSe absorber layer for fabricating CIGSe solar cell. Fig. 10 presents surface morphology of thin film of the third annealing mode; the image shows grain sizes of the CIGSe compound in the range of 200-500 nm, significantly increasing in comparison with the as-synthesized CIGSe nanoparticles. As such, the third annealing mode is most suitable among the three annealing modes tested, even though some voids still exist in thin film. However, this is the nature of the method, which prepared the ink solution based thin film.

The thin film annealed with the third annealing mode was characterized with XRD to confirm the structure of CIGSe compound. Fig. 11 shows that the XRD pattern of CIGSe compound was obtained as expected. Some other peaks also appeared, indicating the presence of Mo substrate and $MoSe_2$ phase forming in the annealing process. However, the formation of a $MoSe_2$ layer at the back interface between CIGSe thin film and Mo substrate under a selenium atmosphere has been reported in the literature [46-48]. The presence of $MoSe_2$ layer is beneficial for an increase in ohmic contact at the CIGSe/Mo back interface, and it also supports the adhesion of the CIGSe layer on the underlying back contact [49-52].

Hall effect was measured with magnetic field intensity of 0.32 T and current of 0.0021 mA. The result showed that the as-prepared CIGSe absorber layer exhibited p-type conductivity with hole concentration (n_p) of 7.876×10^{17} cm^{-3}, the carrier mobility (μ) of 22.2 cm^2/V-s and resistivity (ρ) of 0.3574 ohm-cm.

The optical property of the annealed CIGSe thin film was analyzed by UV-Vis-NIR spectroscopy. The bandgap energy (E_g) value was evaluated from the measured transmittance spectra data by using Tauc's relation:

$$\alpha\cdot h\nu = A\cdot(h\nu - E_g)^{1/2}$$

where α is the absorption coefficient, $h\nu$ is the photon energy. In Fig. 11, the band gap energy of the film was estimated about ~1.3-1.4 eV by extrapolating $(\alpha\cdot h\nu)^2$ vs $h\nu$ plot. This value is close to the $CuIn_{0.7}Ga_{0.3}Se_2$ compound in the literature.

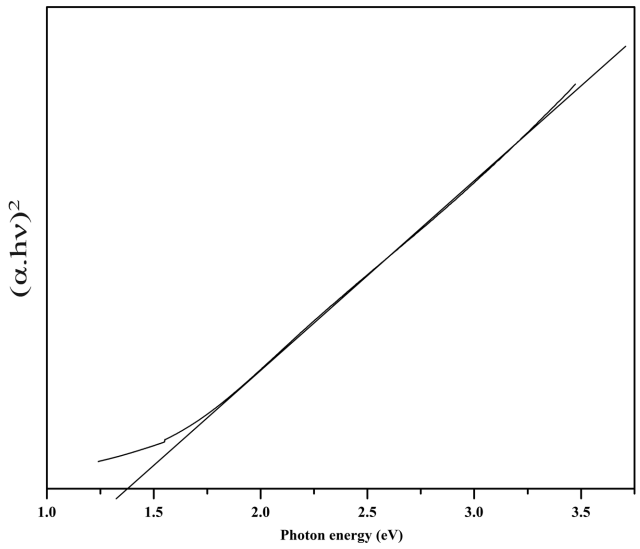

Fig. 12. Plot of $(\alpha h\nu)^2$ versus photon energy hν of CIGSe thin film after being annealed with the third annealing mode.

CONCLUSIONS

CIGSe thin films were prepared by spin-coating method using a greener procedure with ethanol solvent for synthesis of the CIGSe nanocrystals and solvent mixture of 2-propanol and 2-methoxyethanol for the stable ink solution as a dispersion medium. The films annealed with temperature program-90 °C in the first 10 min, 215 °C in the next 10 min and 500 °C in the last 40 min were realized that the grain size and density improved dramatically. The results obtained from characterizations by X-ray diffraction, Raman, XPS, SEM, TEM, ICPS, Hall Effect and UV-Vis revealed that the thin films possess typical tetragonal crystalline structure and similar band gap to those reported for CIGSe thin film. The thickness of the film was around 1 μm, which is in range of thickness of absorber layer for fabricating CIGSe thin film solar cells.

ACKNOWLEDGEMENTS

This work was supported by the Korea Institute of Energy Technology Evaluation and Planning (KETEP) and the Ministry of Trade, Industry & Energy (MOTIE) of the Republic of Korea (No. 20173010012980).

REFERENCES

1. A. Miller, A. Mackinnon and D. Weaire, *Solid State Phys.*, **36**, 119 (1982).
2. R. Baier, Ph.D. Thesis, Helmholtz-zentrums berlin-berichte (2012).
3. https://www.pv-magazine.com/2019/01/21/solar-frontier-hits-new-cis-cell-efficiency-record/.
4. G. Chen, J. Yang, Y. Chan, L. Yang and W. Huang, *Sol. Energy Mater. Sol. Cells*, **93**, 1351 (2009).
5. A. Ihlal, K. Bouabid, D. Soubane, M. Nya, O. Ait-Taleb-Ali, Y. Amira, A. Outzourhit and G. Nouet, *Thin Solid Films*, **515**, 5852 (2007).
6. V. Garg, B. S. Sengar, P. Sharma, A. Kumar, Aaryashree, S. Kumar and S. Mukherjee, *Solar Energy*, **174**, 35 (2018).
7. B. Ayachi, T. Aviles, J. Vilcot, C. Sion and P. Miska, *Thin Solid Films*, **660**, 175 (2018).
8. Z. Yu, C. Yan, Y. Yan, Y. Zhang, T. Huang, W. Huang, S. Li, L. Liu, Y. Zhang and Y. Zhao, *Appl. Surf. Sci.*, **258**, 8527 (2012).
9. M. A. Contreras, K. Ramanathan, J. AbuShama, F. Hasoon, D. L. Young, B. Egaas and R. Noufi, *Prog. Photovolt: Res. Appl.*, **13**, 209 (2005).
10. I. Repins, M. A. Contreras, B. Egaas, C. DeHart, J. Scharf, C. L. Perkins, B. To and R. Noufi, *Prog. Photovolt: Res. Appl.*, **16**, 235 (2008).
11. M. Powalla, P. Jackson, W. Witte, D. Hariskos, S. Paetel, C. Tscham-

ber and W. Wischmann, *Solar Energy Mater. Solar Cells*, **119**, 51 (2013).
12. A. Drici, M. Mekhnache, A. Bouraoui, A. Kachouane, J. C. Bernède, A. Amara and M. Guerioune, *Mater. Chem. Phys.*, **110**, 76 (2008).
13. T. Drobiazg, L. Arzel, A. Donmez, P. Zabierowski and N. Barreau, *Thin Solid Films*, **582**, 47 (2015).
14. R. Caballero, V. Izquierdo-Roca, X. Fontane, C. A. Kaufmann, J. Alvarez-Garcia, A. Eicke, L. Calvo-Barrio, A. Perez-Rodriguez, H. W. Schock and J. R. Morante, *Acta Mater.*, **58**, 3468 (2010).
15. M. Singh, J. Jiu, T. Sugahara and K. Suganuma, *Thin Solid Films*, **565**, 11 (2014).
16. J. Lopez-García, H. Xie, V. Izquierdo-Roca, D. Sylla, X. Fontane, M. Blanes-Guardia, F. Ramos, M. Espindola-Rodriguez, S. Lopez-Marino, E. Saucedo and A. Perez-Rodriguez, *Mater. Chem. Phys.*, **160**, 237 (2015).
17. T. Wada, Y. Matsuo, S. Nomura, Y. Nakamura, A. Miyamura, Y. Chiba, A. Yamada and M. Konagai, *Phys. Stat. Sol.*, **203**, 2593 (2006).
18. M. G. Panthani, V. Akhavan, B. Goodfellow, J. P. Schmidtke, L. Dunn, A. Dodabalapur, P. F. Barbara and B. A. Korgel, *J. Am. Chem. Soc.*, **130**, 16770 (2008).
19. M. Pscherer, M. Gunthner, C. A. Kaufmann, A. Rahm and G. Motz, *Solar Energy Mater. Solar Cells*, **132**, 296 (2015).
20. D. Zhao, Q. Tian, Z. Zhou, G. Wang, Y. Meng, D. Kou, W. Zhou, D. Pan and S. Wu, *J. Mater. Chem. A*, **3**, 19263 (2015).
21. J.-J. Park, J.-G. Lee, D.-Y. Kim, J.-H. Lee, J. H. Yun, J. Gwak, Y.-J. Eo, A. Cho, M. T. Swihart, S. S. Al-Deyab, S. Ahn, D.-H. Kim and S. S. Yoon, *Acta Mater.*, **123**, 44 (2017).
22. J.-J. Park, J.-G. Lee, S. C. James, S. S. Al-Deyab, S. Ahn and S. S. Yoon, *Comput. Mater. Sci.*, **101**, 66 (2015).
23. H. S. Choi, E. Choi, A. Kim, S. P. Yoon and S. G. Pyo, *Phys. Status Solidi A*, **211**, 1877 (2014).
24. G. S. Park, S. J. Park, J. S. Jeong, V. B. Chu, Y. J. Hwang and B. K. Min, *Thin Solid Films*, **621**, 70 (2017).
25. J. Bi, L. Yao, J. Ao, S. Gao, G. Sun, Q. He, Z. Zhou, Y. Sun and Y. Zhang, *J. Power Sources*, **326**, 211 (2016).
26. S. Rampino, M. Bronzoni, L. Colace, P. Frigeri, E. Gombia, C. Maragliano, F. Mezzadri, L. Nasi, L. Seravalli, F. Pattini, G. Trevisi, M. Motapothula, T. Venkatesan and E. Gilioli, *Solar Energy Mater. Solar Cells*, **133**, 82 (2015).
27. M. Kaelin, D. Rudmann, F. Kurdesau, H. Zogg, T. Meyer and A. N. Tiwari, *Thin Solid Films*, **480-481**, 486 (2005).
28. D. Lee, Y. Choi and K. Yong, *J. Cryst. Growth*, **312**, 3665 (2010).
29. F. Huang, A.-H. Yan, H. Zhao, Z. Li, X.-P. Cai, Y.-H. Wang, Y.-C. Wu, S.-B. Yin and Y.-H. Qiang, *Cryst. Res. Technol.*, **49**, 953 (2014).
30. Y.-C. Wang, Y.-T. Yen, C.-H. Liu, C.-H. Chen, W.-C. Kuo, J.-Y. Juang, C.-H. Lai and Y.-L. Chueh, *Thin Solid Films*, **546**, 347 (2013).
31. M. Latha, R. Aruna Devi and S. Velumani, *Opt. Mater.*, **79**, 450 (2018).
32. J. H. Cha, S. J. Noh and D. Y. Jung, *ChemSusChem*, **8**, 2407 (2015).
33. J. H. Lee, J. Chang, J.-H. Cha, Y. Lee, J. E. Han, D.-Y. Jung, E. C. Choi and B. Hong, *Eur. J. Inorg. Chem.*, **5**, 647 (2011).
34. I. Repins, M. A. Contreras, B. Egaas, C. DeHart, J. Scharf, C. L. Perkins, B. To and R. Noufi, *Prog. Photovolt: Res. Appl.*, **16**, 235 (2008).
35. P. Jackson, D. Hariskos, E. Lotter, S. Paetel, R. Wuerz, R. Menner, W. Wischmann and M. Powalla, *Prog. Photovoltaics*, **19**, 894 (2011).
36. I. Repins, M. A. Contreras, B. Egaas, C. DeHart, J. Scharf, C. L. Perkins, B. To and R. Noufi, *Prog. Photovolt: Res. Appl.*, **16**, 235 (2008).
37. T. T. T. Le, T. V. Vu, H. Kim, D.-S. Jeong, B. Pejjai, N. T. N. Truong and C. Park, *Mater. Chem. Phys.*, **207**, 522 (2018).
38. H. Tanino, H. Deai and H. Nakanishi, *Jpn. J. Appl. Phys. Suppl.*, **32-33**, 436 (1993).
39. W. Witte, R. Kniese, A. Eicke and M. Powalla, Proceedings of the fourth IEEE World Conference on Photovoltaic Energy Conversion (WCPEC-4), Waikoloa, USA, 553 (2006).
40. M. C. Biesinger, L. W. M. Lau, A. R. Gerson and R. St. C. Smart, *Appl. Surf. Sci.*, **257**, 887 (2010).
41. C. D. Wagner, A. V. Naumkin, A. Kraut-Vass, J. W. Allison, C. J. Powell and J. R. Jr. Rumble, NIST Standard Reference Database 20, Version 3.4 (web version) (http:/srdata.nist.gov/xps) (2003).
42. J. F. Moulder, W. F. Stickle, P. E. Sobol and K. D. Bomben, Handbook of X-Ray Photoelectron Spectroscopy, Perkin-Elmer Corporation, Physical Electronics Division, Eden Prairie, Minn. (1992).
43. D. Cahen, P. J. Ireland, L. L. Kazmerski and F. A. Thiel, *J. Appl. Phys.*, **57**, 4761 (1985).
44. L. Vegard, *Zeitschrift für Physik*, **5**, 17 (1921).
45. A. R. Denton and N. W. Ashcroft, *Phys. Rev. A.*, **43**, 3161 (1991).
46. D. Abou-Ras, D. Mukherji, G. Kostorz, D. Bremaud, M. Kalin, D. Rudmann, M. Dobeli and A. N. Tiwari, *Mater. Res. Soc. Symp. Proc.*, **865**, F8.1.1 (2005).
47. D. Abou-Ras, G. Kostorz, D. Bremaud, M. Kalin, F. Kurdsau, A. N. Tiwari and M. Dobeli, *Thin Solid Films*, **480**, 433 (2005).
48. R. Krishnan, E. A. Payzant, R. K. Acnyzki, U. Schoop, J. Britt, R. Noufi and T. J. Anderson, Proceedings of the 35th IEEE PVSC Honolulu, 1006 (2010).
49. T. Eisenbarth, T. Unold, R. Caballero, C. A. Kaufmann and H.-W. Schock, *J. Appl. Phys.*, **107**, 034509 (2010).
50. T. Wada, N. Koraha, S. Nishiwaki and T. Negami, *Thin Solid Films*, **387**, 118 (2001).
51. R. Caballero, C. A. Kaufmann, T. Eisenbarth, A. Grimm, I. Lauermann, T. Unold, R. Klenk and H.-W. Schock, *Appl. Phys. Lett.*, **96**, 092104 (2010).
52. R. Caballero, M. Nichterwitz, A. Steigert, A. Eicke, I. Lauermann, H. W. Schock and C. A. Kaufmann, *Acta Mater.*, **63**, 54 (2014).